

## Controlling gap plasmons with quantum resonances

D. C. Marinica,<sup>1</sup> V. M. Silkin,<sup>2,3,4</sup> A. K. Kazansky,<sup>2,3,4</sup> and A. G. Borisov<sup>1,\*</sup>

<sup>1</sup>*Institut des Sciences Moléculaires d'Orsay (ISMO), UMR 8214, CNRS, Université Paris Sud, Université Paris-Saclay, bât 520, F-91405 Orsay, France*

<sup>2</sup>*Donostia International Physics Center (DIPC), Paseo de Manuel Lardizabal 4, 20018 Donostia-San Sebastián, Spain*

<sup>3</sup>*Departamento de Física de Materiales UPV/EHU, Facultad de Ciencias Químicas, University of the Basque Country UPV/EHU, Apto. 1072, 20080 Donostia-San Sebastián, Spain*

<sup>4</sup>*IKERBASQUE, Basque Foundation for Science, 48013 Bilbao, Spain*



(Received 7 May 2018; revised manuscript received 26 August 2018; published 17 October 2018)

We use classical electrodynamics, time-dependent density functional theory, and random-phase approximation to study the gap plasmons propagating in the nm-wide gap between metal surfaces. Particular emphasis is given to the quantum effects emerging when the junction is functionalized with a nanostructure supporting unoccupied gap localized electronic states. With the example of a quantum well (QW) introduced in the junction we show that the optically assisted electron transport across the junction via the gateway QW localized electronic states might strongly affect the lifetime and the propagation length of the gap plasmon. The coupling to the single-particle electron-hole excitations from occupied electronic states at metal surfaces into the QW-localized electronic states provides an efficient decay channel of the gap plasmon mode. Different from the through-gap electron tunneling discussed in the plasmonics literature, the electron transport involving the gateway electronic state is characterized by the threshold behavior with plasmon frequency. As a consequence, the dynamics of the gap plasmon can be controlled by varying the binding energy of the QW-localized electronic state. In more general terms, our results demonstrate strong sensitivity of the gap plasmons to the optically assisted electron transport properties of the junction which opens further perspectives in design of nanosensors and integrated active optical devices.

DOI: [10.1103/PhysRevB.98.155426](https://doi.org/10.1103/PhysRevB.98.155426)

### I. INTRODUCTION

Interaction between electromagnetic field and collective electronic excitations in metals or two-dimensional (2D) materials, plasmons, allows one to reach orders of magnitude field enhancement and to manipulate the light at the scale well below the wavelength. This opens a broad range of applications placing plasmonics at the focus of intense research effort [1–5]. Plasmonic excitations in individual (nano)objects, in engineered nanostructures, and at surfaces can be divided in two major classes: propagating and localized plasmons. Propagating plasmons are characterized by continuous spectrum with an energy dispersion given by the wave vector, while the localized plasmons are characterized by a discrete energy spectrum defined by a set of quantum numbers. Obviously, quantization of the propagating plasmons by, e.g., reflecting boundary conditions also leads to their localization and the discrete energy spectrum emerges as in an optical corrals [6,7], planar nanoparticles [8,9], and patch antennas [10–17].

Among the examples above, the gap plasmons (GPs) propagating in a narrow dielectric layer sandwiched between metal surfaces are of great practical interest ranging from information transfer technologies to sensing and single-photon sources. This is because the GPs allow one to reach strong field confinement, low losses, and high effective index of re-

fraction [18–25]. In this context, the gap plasmon waveguides have been proposed for plasmonic circuitry [26–29]. The GP modes localized in the junction between a metal nanoparticle and a metal surface determine the optical response of the patch nanoantenna [10–17]. As well, the excitation of the localized GP modes is often evoked as an important mechanism for tip enhanced Raman scattering [30–32], or for the light sources based on the tunneling junctions [33–36]. Recent experimental developments demonstrated the excitations of the (single) molecules placed in plasmonic nanocavities. The coupling between GPs and molecular excitons drives in this case molecular optomechanics [37–43] as well as the light emission from molecule functionalized gaps [44–52].

Interpretation of the experimental data on the plasmon coupling with molecular excitons in narrow gaps between metal surfaces requires definition of the relevant plasmon modes. Typically, these are obtained using local classical electrodynamics calculations [37–43], and are then used within the framework of the cavity quantum electrodynamics, or within the framework of classical theory. At the same time, reaching the nm size of the molecule functionalized plasmonic gaps puts forward a question on the role of the quantum effects such as nonlocality and electron tunneling. The latter might be affected by electronic transitions involving the orbitals localized on the molecular species in the gap.

The effect of the nonlocal screening on the propagation of the GP has been studied using the hydrodynamic model. In brief, for the noble metals the nonlocality results in an

\*andrei.borisov@u-psud.fr

effective refraction index lower than that predicted by the classical local theory [21–25]. The divergence of the effective refraction index at vanishing sizes of the gap is removed. Indeed, neglecting the retardation effects, within the classical local Drude description of the metal dielectric function the dispersion of the GP is given by [53]  $\omega_{\text{GP}} \sim \omega_p \sqrt{k D_g}$ . Here,  $\omega_{\text{GP}}$  and  $k$  are the energy of the GP and its wave vector,  $\omega_p$  is the bulk plasma frequency, and  $D_g$  is the width of the gap between metal surfaces. When the nonlocal effects are taken into account, the screening charges are located not at the geometrical surfaces, but shifted inside metal so that  $D_g$  effectively increases [54–56].

Along with nonlocal screening, a number of experimental and theoretical studies demonstrated that the electron tunneling can strongly affect the plasmon modes of the metal nanostructures with narrow gaps [57–66]. However, the effect of the electron tunneling on the propagating GP has not been addressed in detail so far, in particular for the functionalized gaps where the photon assisted electron transport (PAT) through the gateway electronic states localized in the gap region becomes possible [67–75]. Such unoccupied electronic states might be the lowest unoccupied molecular orbitals (LUMO) of the molecules bridging the junction, or the quantized states of the quantum well structures, as considered in this work. Different from the situation where the electrons tunnel through the vacuum potential barrier separating the nanostructures [57–66], the PAT through the gateway gap-localized electronic states is characterized by the frequency threshold. This frequency threshold corresponds to the onset of electronic transitions from the Fermi levels of the metal leads into the gap-localized states. It is worth noting that the existence of the tunneling at optical frequencies for the functionalized plasmonic gaps is confirmed by the observation of the optical rectification in these systems [76,77].

In this work, using classical electrodynamics, density functional theory (DFT), time-dependent density functional theory (TDDFT), and random-phase approximation (RPA), we study energy dispersion and decay of the GP in nanogaps between metal surfaces functionalized with a quantum well structure. Our results demonstrate that, because of the localization of the electric field in the gap region, the GPs with frequencies above the threshold value  $\omega_{\text{th}}$  efficiently induce PAT across the quantum well (QW) functionalized junction. The PAT is dominated by the transitions involving unoccupied quantum-well localized electronic states (QWSs). The associated electron-hole excitations from the occupied electronic states of the metal leads to the unoccupied gateway QWSs serve as an efficient decay channel of the GPs. This is to be compared with decay of the surface plasmon via electron-hole excitations inside metal [53,66,78–82]. As a result, we obtain that the GP lifetime and propagation length can be strongly reduced for the frequencies above  $\omega_{\text{th}}$ . In this respect, controlling the  $\omega_{\text{th}}$  value via tuning the energies of the gap-localized states with, e.g., a gate electrode, opens up the possibility of active electrical control of the GP propagation length with possible application for active optical devices based on the gap plasmon circuitry. We also discuss the quantum-classical correspondence of this result and the role of the strength of the electronic coupling between the gap-localized electronic states and the metal leads.

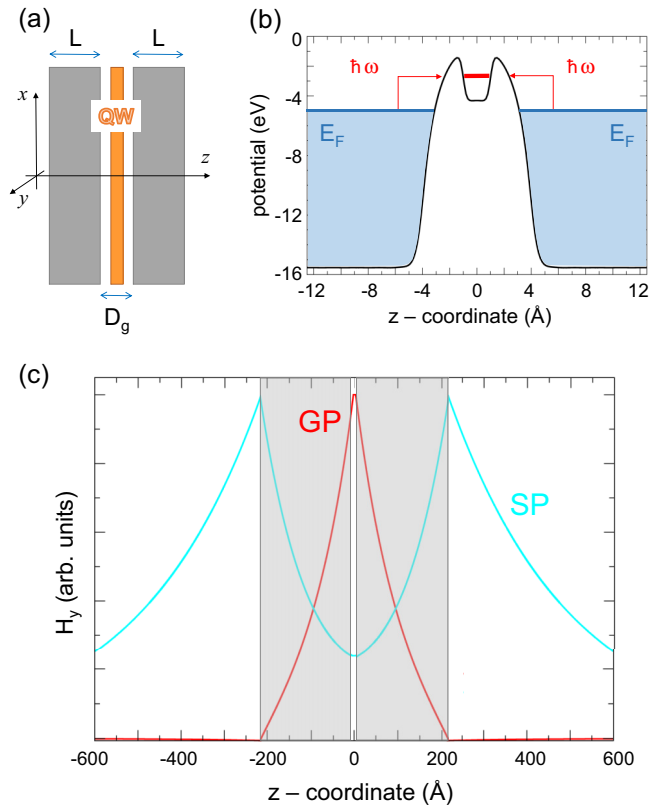


FIG. 1. (a) The geometry of the studied system. Two parallel metal slabs of width  $L$  are separated by a vacuum gap of width  $D_g$ . The gap is functionalized with a QW structure placed at its middle. The coordinate system is set such that the  $z$  axis is perpendicular to the slabs and the  $(x, y)$  plane is parallel to the slab surfaces. (b) The one-electron potential in the gap region is plotted as a function of the  $z$  coordinate perpendicular to the metal surface along with electronic structure corresponding to the 1D motion in the  $z$  direction. The zero energy corresponds to the vacuum level. Shaded regions indicate the occupied electronic states of the metal slabs below the Fermi levels ( $E_F$ ) shown with thick blue lines. Thick red line shows an unoccupied quantum well state. The electronic transitions involved in the PAT are schematically shown with red arrows. (c) Magnetic field of the plasmon modes characterized by symmetric with respect to the middle of the gap  $H_y$  component of the magnetic field. Gap plasmon (GP) and hybridized surface plasmon (SP) are shown.

The paper is organised as follows. In Sec. II we describe the studied system and the methods used. Section III is devoted to the results of this work and their discussion. Sec. IV provides summary and conclusions. Atomic units are used throughout the paper unless otherwise stated.

## II. METHODS

### A. System and general considerations

As stated in the Introduction, we are interested in how the dynamics of the GP is affected by the PAT through the unoccupied electronic states induced by the functionalization of the junction between metallic surfaces. To this end we study the structure schematically shown in Fig. 1(a). The junction consists of two identical metal slabs of width  $L$  separated

by a narrow gap of width  $D_g \sim 1$  nm. Results presented in this paper are obtained with  $L \sim 20$  nm. In order to check robustness of the main qualitative and quantitative trends we also performed calculations with  $L \sim 10$  nm and  $L \sim 5$  nm. Thicker slabs would require prohibitively long RPA and TDDFT calculations. The gap is functionalized with a metallic QW structure formed by a metal film of several monolayers width [83,84] isolated from the leads by a dielectric. Similar multilayer metal-dielectric-metal structures are used as optical metamaterials or waveguide claddings [85–87] in the infrared and visible frequency ranges; as well, they are used for the XUV optics [88,89].

The metal-QW-metal structure is translationally invariant in the  $x$  and  $y$  directions. The  $z$  direction is perpendicular to the interfaces. The QW electron motion is confined in the  $z$  direction leading, within the 1D picture, to the unoccupied QW-localized electronic state at energy  $E_0$ . This state can be populated by the electrons from the Fermi levels of the leads by absorption of photons within the eV energy range as sketched in Fig. 1(b). We consider the case where the transitions from the occupied QW states require higher photon energies and can be neglected. The model outlined here should also be relevant for the systems where the narrow plasmonic gap between metal nano-objects is functionalized with an organic self-organized molecular layer as has recently been studied in several works [44–52,90–92]. In this case, if the energy difference between the highest occupied molecular orbital (HOMO) and LUMO is large enough, the optical transitions from HOMO are not active within the frequency range of interest corresponding to the electron excitation energy from the Fermi level of the slabs to LUMO.

In what follows, the dielectric spacer layers between the QW and metal slabs are considered as vacuum. The electron interaction with the metal slabs is obtained self-consistently using the DFT calculations within the free-electron approximation. The QW structure is represented with model potential, as described below in this section. The thickness of the spacer layers at the metal/QW interfaces is set such that the metal slabs are electronically decoupled in the absence of the QW (the tunneling across the vacuum gap is negligible). At the same time, for the functionalized gap, the QWS is strongly coupled to the metal leads and appears as a broad unoccupied resonance in the projected density of electronic states. Thus, it can serve as an efficient intermediate for the electron transport across the junction. From technological considerations one would expect that the spacer layer between the QW and metal leads is formed by an oxide film or other dielectric material. We address this issue after the discussion of the main results and the underlying physics which show that our main conclusions are robust with respect to the approximations used.

The system of two metal slabs with narrow vacuum gap supports four propagating plasmon modes [10,18]. Without loss of generality we will consider the wave vector  $k$  to be directed along the  $x$  axis. These modes possess the electric-field components along the  $x$  axis ( $\mathcal{E}_x$ ) and the  $z$  axis ( $\mathcal{E}_z$ ), and can be classified according to the symmetric/antisymmetric character of the magnetic field  $H_y$  with respect to the middle of the gap ( $z = 0$ ). The magnetic fields of the symmetric modes are shown in Fig. 1(c). One can distinguish the gap

plasmon (GP, red line) localized essentially in the gap and the hybridized surface plasmon mode (SP, blue color) resulting from the hybridization of the surface plasmons localized at external surfaces of the slabs. Calculations have been performed for  $k_{GP} = 0.00566 \text{ \AA}^{-1}$  so that  $\omega_{GP} = 1.74 \text{ eV}$  and  $\omega_{SP} = 8.62 \text{ eV}$  as retrieved from the dispersion curves shown below.

When the vacuum gap is functionalized with a QW structure as sketched in Fig. 1, the 2D band of unoccupied QW localized states emerges at energies  $E_0 + \mathbf{q}^2/2$ . Here  $E_0 > E_F$ , and  $\mathbf{q}$  is an electron wave vector parallel to the surface. (For the case of the molecular layer present in the gap the parabolic dispersion should be replaced by the band formed by the hybridization of the LUMO orbitals of individual molecules.) In such a situation, for  $\omega_{GP} \geq \omega_{th} = E_0 - E_F$  the strong electric field of the GP allows for efficient electronic excitations from occupied electronic states of the metal leads to the QWS. The GP triggers the photoassisted transport across the junction [67–75]. Within the classical point of view, the PAT is linked with resistive losses. In quantum-mechanical terms, an efficient absorption of electromagnetic energy occurs when the photon energy matches the energy difference between electronic states coupled by the time-dependent field. Thus, the PAT associated with electron-hole excitations into the QWS would be an additional decay channel for the GP plasmon mode [53,66,78–82]. However, the question to be addressed is whether the presence of the single band of the empty states (single state at  $E_0$  if only the motion perpendicular to the surface is considered) is sufficient to notably alter the dynamics of the GP. We note in passing that because of the field localization at external surfaces of the metal slabs the SP appears nearly unaffected by the electronic properties of the gap region.

## B. Calculation of the plasmon linewidth and propagation length with RPA

To calculate the dynamics of the GP in the metal-QW-metal structure we use the quantum DFT, TDDFT, and RPA approaches, as well as the classical electromagnetic theory. The metal slabs are modelled using free-electron, jellium metal (JM) approximation [93] which well captures the effects owing to high mobility of valence electrons, such as spill out of electron density and tunneling. Within the JM the atomic cores are not treated explicitly, but represented by a positive background charge density  $n^+ = [\frac{4\pi}{3}r_s^3]^{-1}$ . Here,  $r_s$  is the Wigner-Seitz radius. At a price of losing full atomistic details, as well as features in the optical response due to the localized bands (such as  $d$  bands in the case of noble metals), the simplification owing to the JM allows us to address large size systems with well developed plasmon modes. Thus, the quantum effects in plasmonics were predicted [57,58,79,94] using the JM, which in particular allowed a thorough study of the underlying physics. These results were later on confirmed experimentally and theoretically with *ab initio* studies [59–66,95]. In what follows we use  $r_s = 2.07 a_0$  corresponding to an Al metal. The Al is a prototype free-electron metal which fully validates the JM description and allows meaningful straightforward comparison with classical electromagnetic calculations based on the Drude model for the metal permit-

tivity. Moreover, recently Al has attracted growing interest in the context of plasmonic applications [96–100]. We neglect formation of the oxide layer at the surfaces of Al films which would affect the tunneling probability through the gap. It is worthwhile to stress however that, similar to the earlier works on tunneling effects in plasmonics, we use the JM to reveal the robust physical effects and discuss their dependence on the main parameters of the system. We further elaborate on the issue of the model description below in this paper.

As a first step, the ground-state electronic structure of the system is obtained by solving self-consistently the Kohn-Sham (KS) equations of DFT [101]. Considering the free-particle electron motion in the  $(x, y)$  plane, the KS orbitals are sought in the form  $e^{i\mathbf{q}\cdot\mathbf{r}}\psi_j(z)$ , where  $\mathbf{q}$  is the electron wave vector in the  $(x, y)$  plane, and  $\mathbf{r}_{\parallel} = (x, y)$ . The  $\psi_j(z)$  states solve the 1D KS equations,

$$\left[-\frac{1}{2}\frac{d^2}{dz^2} + V_{\text{eff}}(n, z)\right]\psi_j(z) = E_j\psi_j(z), \quad (1)$$

and form a discrete spectrum with energies  $E_j$  because of the reflection at the boundaries of the metal slabs. The electron density of the system  $n(z)$  is given by  $n(z) = \frac{1}{\pi} \sum_{j=1}^N (E_F - E_j) |\psi_j(z)|^2$ , where the spin degeneracy and the translational invariance of the problem are accounted for. The sum runs over occupied ( $j = 1, \dots, N$ ) KS orbitals such that  $E_j \leq E_F$ . Note that each  $z$ -quantized state gives rise to the 2D continuum of electronic states with energies  $E_{\mathbf{q},j} = E_j + q^2/2$ .

The effective one-electron potential is given by several contributions:

$$V_{\text{eff}}(n, z) = V_H(n, z) + V_{\text{xc}}(n, z) + V_{\text{QW}}(z). \quad (2)$$

In Eq. (2),  $V_H$  is the Hartree potential,  $V_{\text{xc}}$  is the exchange correlation potential of Gunnarsson and Lundqvist [102],  $V_{\text{QW}}(z)$  is the model potential which describes an electron interaction with the QW structure. We use  $V_{\text{QW}}(z) = -V_0[1 + \exp(\frac{|z-b|}{\delta})]^{-1}$ , with  $b = 2a_0$  and  $\delta = 0.25a_0$  (the Bohr radius  $a_0 = 0.53 \text{ \AA}$ ). The width of the potential well is thus  $2b \sim 2 \text{ \AA}$ , and its depth is given by the  $V_0$  parameter. Typically, the  $2 \text{ eV} \leq V_0 \leq 5 \text{ eV}$  range is encompassed in our study, and variation of  $V_0$  can be seen as the effect of applying voltage to a gate electrode. The above choice of the QW model allows one to introduce the unoccupied quantum well localized electronic state between the vacuum level and the Fermi levels of the slabs [see Fig. 1(b)] with binding energy controlled by the potential depth  $V_0$ .

In Fig. 2 we show the QW induced resonance in the energy dependence of the projected density of states (PDOS) for various values of  $V_0$  and two widths of the junction  $D_g = 8 \text{ \AA}$  and  $D_g = 10 \text{ \AA}$ . Because of the planar symmetry of the problem, only the electron motion perpendicular to the metal surface is considered here. The PDOS has been calculated from the solution of the one-electron time-dependent Schrödinger equation using the wave-packet propagation approach [103]. The initial wave function is set as  $\varphi_0 = A \exp[-(\frac{z-2}{2.5})^2]$ , where  $A$  is the normalization constant. Absorbing boundary conditions are introduced inside metal so that the electron reflections at distant metal/vacuum interfaces are suppressed.

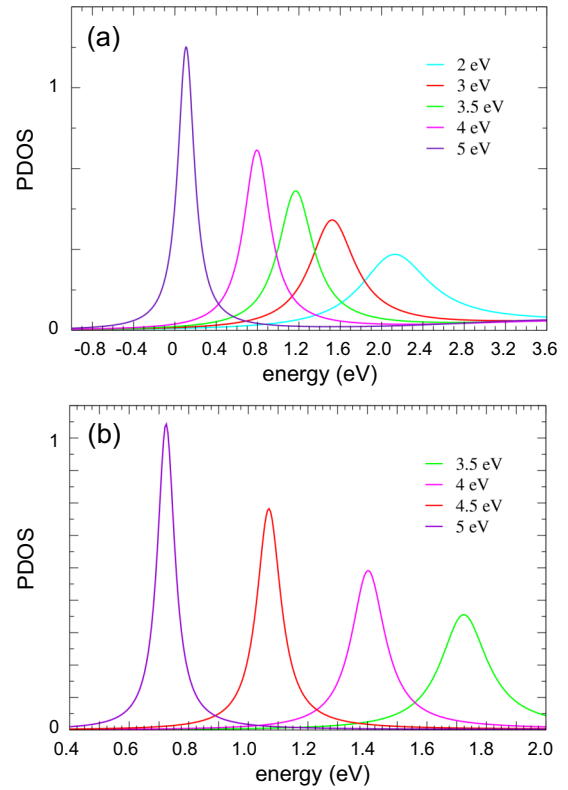


FIG. 2. QW structure in the vacuum gap between semi-infinite Al slabs. (a) An unoccupied QW resonance in the projected density of electronic states for the zero electron momentum parallel to the surface, and for various values of the depth of the QW potential  $V_0$  as given in the insets. The results are shown (in arbitrary units) as functions of the electron energy measured from the Fermi level of Al metal. The width of the gap  $D_g = 8 \text{ \AA}$ . (b) Same as panel (a) but for the width of the gap  $D_g = 10 \text{ \AA}$ .

Results then correspond to the functionalized gap between semi-infinite metal leads. In this situation, the QWS induced resonance is not quantized by the finite-size effect. It features the Lorentzian profile allowing us to determine the energy  $E_0$  of the quasistationary QWS and its width  $\Gamma$ . The latter corresponds to the rate of the QWS population decay (inverse of the lifetime) via energy-conserving one-electron transfer into the metal leads at fixed value of the electron wave vector parallel to the surface.

As a general trend, for the fixed width of the gap  $D_g$ , increasing the depth of the QW potential  $V_0$  lowers the energy of the QWS. The energy in Fig. 2 is measured from the Fermi level of metal slabs, so that one can easily infer the  $V_0$  dependence of the gap plasmon frequency threshold for an efficient PAT between Al slabs via an intermediate of the QWS. Since the potential at the QW/metal interfaces is only slightly modified by changing  $V_0$ , the effective barrier for the electron tunneling into the metal increases for lower  $E_0$ . The quasistationary QWS becomes longer-lived and the resonance width  $\Gamma$  decreases. Similarly, increasing  $D_g$  [cf. Figs. 2(a) and Fig. 2(b)] at fixed width of the QW leads to broader QW/metal potential barriers. The decay rate  $\Gamma$  of the QWS decreases leading to narrower resonances in PDOS. Note that increasing  $D_g$  at a fixed value of  $V_0$  reduces an attractive part of the



electron-metal interaction potential at the position of the QW. The QWS resonance shifts then to somewhat higher energies.

To calculate the effect of the QWS resonance on the dynamics of the GP mode we use the RPA approach which is the linear-response approximation to the full TDDFT. In a system like that studied here the rate of electronic excitations created by an external potential of the form

$$V^{ext}(z; k, \omega) = -\frac{2\pi}{k} e^{kz} \quad (3)$$

is proportional to the imaginary part of the surface response function  $\text{Im}[g(k, \omega)]$ , where  $k$  stands for the absolute value of the momentum parallel to the surface. The surface response function is determined as [104]

$$g(k, \omega) = -\frac{2\pi}{k} \int dz \int dz' e^{k(z+z')} \chi(z, z'; k, \omega). \quad (4)$$

Here  $\chi(z, z'; k, \omega)$  is the 2D Fourier transform of the dynamical density-response function of interacting electrons  $\chi(\mathbf{r}, \mathbf{r}'; \omega)$  which is a nonlocal and complex function. In the framework of TDDFT  $\chi(\mathbf{r}, \mathbf{r}'; \omega)$  satisfies the integral equation

$$\chi = \chi^0 + \chi^0(V + K_{xc})\chi \quad (5)$$

with  $\chi^0(\mathbf{r}, \mathbf{r}'; \omega)$  being the density-response function of non-interacting electrons,  $V(\mathbf{r} - \mathbf{r}')$  is the Coulomb potential, and  $K_{xc}(\mathbf{r}, \mathbf{r}'; \omega)$  accounts for dynamical exchange-correlation effects. In the RPA used here  $K_{xc} = 0$ . With the eigenfunctions  $\psi_j(z)$  and eigenenergies  $E_j$  obtained in the ground-state DFT calculation we evaluate the 2D Fourier transform  $\chi^0(k, z, z', \omega)$  for the system under study as

$$\chi^0(z, z'; k, \omega) = \frac{2}{A} \sum_{i,j} \psi_i(z) \psi_j(z) \psi_i(z') \psi_j(z') \times \sum_{\mathbf{q}} \frac{f_{\mathbf{q},i} - f_{\mathbf{q}+\mathbf{k},j}}{E_{\mathbf{q},i} - E_{\mathbf{q}+\mathbf{k},j} + \omega + i\eta}. \quad (6)$$

Here the sum over the  $i$  and  $j$  bands includes all occupied and the unoccupied states up to a maximal energy of 150 eV above the Fermi level;  $A$  is the area of the surface supercell. The Fermi factors  $f_{\mathbf{q},j}$  are taken at zero temperature and  $\eta$  is a positive infinitesimal. Further details of calculation of  $\chi^0$  and  $\chi$  can be found in Refs. [105,106].

Once the loss function  $\text{Im}[g(k, \omega)]$  is calculated in the  $(k, \omega)$  plane, the plasmon modes appear as resonance features allowing one to obtain their frequency dispersion  $\omega_{\text{GP}}(k)$ , as well as their lifetime  $\tau$  and propagation length  $\ell$ . The lifetime  $\tau$  of the GP mode with defined momentum parallel to the surface  $k$  is given by the inverse of the energy width of the GP resonance  $\tau = (\Delta\omega)^{-1}$ , where  $\Delta\omega$  is obtained from the frequency dependence of the resonance profile in the loss function at fixed  $k$ . The propagation length  $\ell$  of the GP excited, e.g., by a spatially localized monochromatic source is of relevance for plasmonic circuitry. It is given by the inverse of the GP momentum broadening  $\ell = (\Delta k)^{-1}$ , where  $\Delta k$  is obtained from the wave-vector dependence of the resonance in the loss function at fixed frequency  $\omega$ .

### C. Calculation of the plasmon linewidth and propagation length with classical electromagnetic theory

In order to get a simple physical insight into the main factors controlling the dynamics of GP in functionalized nanogaps, the results of quantum RPA calculations are compared with predictions of the local classical electromagnetic theory. The GP is characterized by the field components  $\mathcal{E}_x$ ,  $\mathcal{E}_z$ , and  $H_y$ . Assuming the  $e^{-i\omega t} e^{ikx}$  dependence of the fields on time and on the parallel to the surface coordinates, we obtain from classical Maxwell equations ( $\varepsilon$  is the  $z$ -dependent dielectric function,  $c$  is the speed of light in vacuum)

$$\mathcal{E}_x = -i \frac{c}{\omega \varepsilon} \partial_z H_y, \quad \mathcal{E}_z = -\frac{c}{\omega \varepsilon} H_y, \quad (7)$$

and

$$\left[ \partial_z \frac{1}{\varepsilon} \partial_z - \frac{k^2}{\varepsilon} + \frac{\omega^2}{c^2} \right] H_y = 0. \quad (8)$$

Here, without loss of generality we choose the plasmon wave vector  $\mathbf{k}$  to be directed along the  $x$  axis. In what follows we will be interested in plasmon modes possessing symmetric (with respect to the center of the gap) magnetic-field component  $H_y$ . These modes, and in particular GP, allow us to obtain strong gap-localized electric fields leading to the efficient PAT through the junction. Assume that within each region: (i) in the gap ( $g$ ) ( $|z| \leq z_1 \equiv D_g/2$ ), (ii) inside the metal ( $m$ ) ( $z_1 \leq |z| \leq z_2 \equiv D_g/2 + L$ ), and (iii) in the vacuum ( $v$ ) ( $z_2 \leq |z|$ ), the material dielectric function is local and  $z$  independent. Then, the magnetic-field component  $H_y$  can be sought in the form

$$H_y = \begin{cases} a_g e^{-\gamma_g z_1} [e^{-\gamma_g z} + e^{\gamma_g z}], & 0 \leq z \leq z_1. \\ a_m e^{-\gamma_m(z-z_1)} + b_m e^{\gamma_m(z-z_2)}, & z_1 \leq z \leq z_2. \\ a_v e^{-\gamma_v(z-z_2)}, & z_2 \leq z. \end{cases} \quad (9)$$

The exponential factor within each region is given by  $\gamma_s^2 = k^2 - \varepsilon_s \frac{\omega^2}{c^2}$ , where  $s = (g, m, v)$ . For the sake of comparison with RPA results we have also used the nonretarded classical calculations, where  $\gamma_s = k$ .

In the vacuum region  $\varepsilon_v = 1$ . The permittivity of the metal slabs is described with Drude model  $\varepsilon_m = 1 - \frac{\omega_p^2}{\omega(\omega + i\eta)}$  with plasma frequency of Al  $\omega_p = 15.82$  eV, and attenuation  $\eta = 0.19$  eV as determined from the comparison with RPA results for the case of the vacuum gap between metal slabs (metal-vacuum-metal structure). It is worth noting that the parameters of the Drude model reported above are very close to those deduced from the measured Al permittivity within the considered frequency range [96,107,108]. The present value of the attenuation  $\eta$  is however somewhat larger as it accounts for the Landau damping in the present system.

The choice of the dielectric function of the gap material is crucial to reproduce the RPA results. In the case of the nonfunctionalized vacuum gap between metal surfaces we use  $\varepsilon_g = 1$ . For the QW functionalized gaps we assume that the fields are nearly constant in the gap region and employ a local connection between the dielectric function and transport properties of the gap:

$$\varepsilon_g = 1 + i \frac{4\pi \sigma(\omega)}{\omega}. \quad (10)$$

The conductivity of the gap  $\sigma(\omega)$  has to account for the electron tunneling effects, and, in particular, for the PAT through the unoccupied QWS. It is then obtained from the TDDFT calculations [109,110] (see details in Ref. [110]) for the  $k = 0$  case. This approximation is justified because the optical wave vectors addressed in this work are nearly two orders of magnitude smaller than the Fermi wave vector of Al electrons. The complex frequency-dependent conductivity of the junction is defined as  $\sigma(\omega) = J_z(\omega)/\mathcal{E}_z(\omega)$ , where  $J_z(\omega)$  and  $\mathcal{E}_z(\omega)$  are the  $z$ -components of the current and electric field at the middle of the junction. Thus, the classical local approach (we refer to it as classical model below) accounts for the ac transport properties of the junction through the quantum TDDFT inputs. It is noteworthy that, because of the high symmetry, the TDDFT calculations with  $z$ -polarized electromagnetic pulse are  $\sim 10^2$  times faster than the full RPA run over the  $(k, \omega)$  range of interest.

Using boundary conditions for the fields at the gap/metal ( $z_1 = D_g/2$ ) and metal/vacuum ( $z_2 = D_g/2 + L$ ) interfaces Eq. (9) leads to the homogeneous system of linear equations for  $a_s$  and  $b_s$  coefficients [ $s = (g, m, v)$ ] which has a solution if

$$\det(\mathbb{R}) = 0, \quad (11)$$

where

$$\mathbb{R} = \begin{pmatrix} -e^{-\gamma_g D_g} + 1 & 1 & e^{-\gamma_m L} & 0 \\ 0 & e^{-\gamma_m L} & 1 & -1 \\ \frac{\gamma_g \varepsilon_m}{\gamma_m \varepsilon_g} [e^{-\gamma_g D_g} - 1] & -1 & e^{-\gamma_m L} & 0 \\ 0 & e^{-\gamma_m L} & -1 & \frac{\gamma_v \varepsilon_m}{\gamma_m \varepsilon_v} \end{pmatrix}. \quad (12)$$

Equation (11) determines the dispersion of the plasmon modes with even symmetry of  $H_y$ . In practice, we analyze the resonances of the  $|1/\det(\mathbb{R})|$  function in the  $(k, \omega)$  plane as shown in Fig. 3 for the case of the vacuum gap between metal slabs. Two resonances corresponding to the hybridized plasmon mode with surface character (SP) and gap plasmon (GP) are obtained. The resonance analysis yields the gap plasmon characteristics: (i) The GP frequency  $\omega_{GP}$  as a function of the wave vector  $k_{GP}$ , i.e., the dispersion relation, (ii) the width of the plasmon resonance  $\Delta\omega$  at fixed  $k_{GP}$  equal to the inverse of the GP lifetime  $\tau$ , and (iii) the  $\Delta k$  broadening at fixed  $\omega_{GP}$  equal to the inverse of the GP propagation length  $\ell$ .

### III. RESULTS AND DISCUSSION

#### A. Dispersion relation

The SP and GP character of the symmetric in  $H_y$  plasmon modes results in their very different dispersion as can be seen in Fig. 3 for the case of the vacuum gap [18]. The hybridized SP closely follows the dispersion of the individual surface plasmon at the metal/vacuum interface  $k_{SP} = \frac{\omega}{c} \sqrt{\frac{\varepsilon_m}{1+\varepsilon_m}}$ . Its wave-vector dependent frequency is close to the light line at low  $k$ , and it approaches the  $\omega_p/\sqrt{2}$  constant value at large  $k$ . The “slow” GP features a very different dispersion curve that can be approximately described with  $\omega_{GP} \sim \omega_p \sqrt{k D_g}$  dependence in the nonretarded limit [53].

In Fig. 4 we plot the GP dispersion calculated using different approaches for the nanostructure characterized by the  $D_g = 8 \text{ \AA}$  gap between  $L = 20 \text{ nm}$  Al slabs. For the vacuum

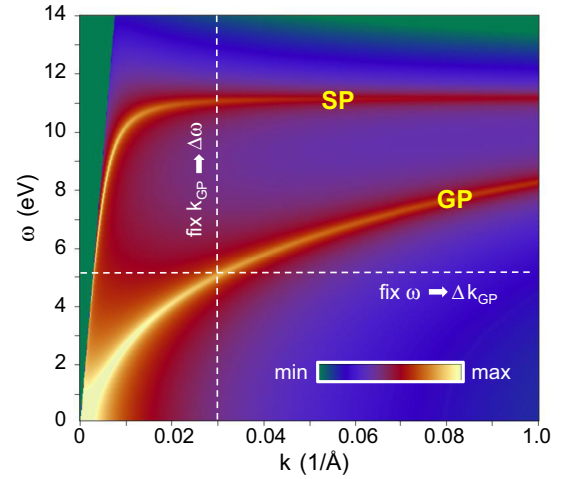


FIG. 3. Dispersion of the symmetric plasmon modes with surface plasmon (SP) and gap plasmon (GP) character. Results of the classical calculations  $\ln[|\det(\mathbb{R})|^{-1}]$  are shown as function of the wave vector  $k$  along  $x$  axis and frequency  $\omega$ . The case of the vacuum gap of the width  $D_g = 8 \text{ \AA}$  gap between  $L = 20 \text{ nm}$  Al slabs is considered. Position of the resonances at  $(\omega, k)$  plane allows extraction of their dispersion characteristics. The cuts at fixed  $k$  or  $\omega$ , indicated with dashed lines, can be used to extract the frequency  $\Delta\omega$  and wave vector  $\Delta k$  width of the plasmon modes, i.e., the plasmon mode lifetime  $\tau = 1/\Delta\omega$  and its propagation length  $\ell = 1/\Delta k$ .

gap, the results obtained with quantum RPA (black dots) and classical theory (solid black line) are very close to each other. However, the RPA predicts slightly higher GP frequencies because it does not account for the retardation effects. This follows from the comparison between RPA and nonretarded (dashed black line) classical calculations. Overall, the clas-

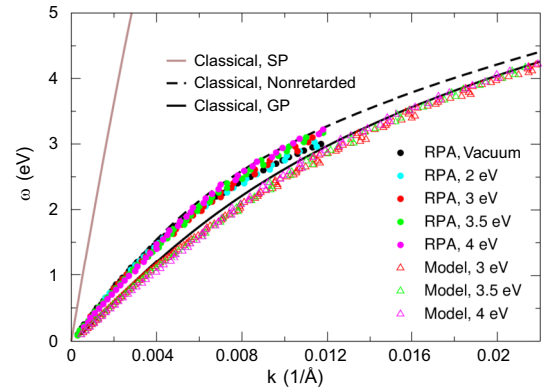


FIG. 4. Dispersion of the plasmon modes with even symmetry of magnetic field  $H_z$ . The wave-vector dependence of the frequency of the surface plasmon (SP) and gap plasmon (GP) is shown for the structure characterized by the  $D_g = 8 \text{ \AA}$  gap between  $L = 20 \text{ nm}$  Al slabs. Results of the classical calculations for the vacuum gap (classical, solid lines) and classical calculations with model dielectric function (model, triangles) for the QW functionalized gap are compared with RPA data (dots). For the QW functionalized gap results obtained with different potential depths of the QW,  $V_0$ , are shown. For further details see the insets. We also show the GP dispersion calculated classically within nonretarded limit for the vacuum gap (dashed line).

sical theory performs remarkably well for these extremely narrow gaps. The direct comparison between quantum and classical calculations for the dispersion of the GP modes presented here sets a benchmark for using local classical theories in the description of the GP modes in nm gaps. The remaining differences we ascribe to the effect of the nonlocal screening [21–25] not captured within the local classical model. Because of the nonlocality the “effective” size of the gap measured between the centroids of the screening charges at opposite surfaces is different from the geometrical size of the gap [54–56]. For the free-electron Al metal the effective size of the gap is smaller than  $D_g$  [54] leading to lower GP energies at fixed  $k$ . For the QW functionalized gap the dispersion curve is only mildly affected in both RPA and classical model calculations. In particular, the change of the depth of the QW potential and thus of the energy of the QWS (see Fig. 2) does not lead to an appreciable change of the  $\omega_{GP}(k)$  dependence. This is in sheer contrast with the lifetime and propagation length of the GP as we discuss below.

### B. RPA calculations of the gap plasmon decay

Within the RPA approach, the GP dispersion, as well as the  $\omega$  and  $k$  broadening of the plasmon line, are obtained from the loss function calculated in the  $(k, \omega)$  plane. Analysis of the results is similar to the classical case where Eq. (11) is used [see discussion of Fig. 3 in Sec. II]. The loss function calculated with RPA for the nanostructure with a  $D_g = 8$  Å gap between  $L = 20$  nm Al slabs is shown in Fig. 5 for the 0–3.5 eV frequency range relevant for optical applications. We compare results obtained for the vacuum gap and the gap functionalized with QW structure of variable potential depth. Depending on the QW potential depth  $V_0$ , the energy  $E_0$  of the bottom of the 2D band of the QWS takes different values (see Fig. 2). In turn, this modifies the frequency onset of the optical excitations from the occupied electronic states below Fermi levels of Al metal slabs into the unoccupied QWS:  $\omega_{th} = E_0 - E_F$ . The small change of the electron wave vector parallel to the surface (accounted for in the RPA calculations) can be neglected here for the sake of simplicity.

When the QW is introduced in the junction, the width of the GP resonance strongly increases above the threshold frequency  $\omega_{GP} \geq \omega_{th}$ . The GP lifetime and propagation length are reduced. Owing to the electric-field localization in the junction between metal surfaces, the GP is strongly coupled with and efficiently decays to the single-particle electron-hole pair excitations from the metal slabs into the unoccupied QWS. Such plasmon decay into electrohole pair excitations [53,66,78–82] is often evoked in the context of hot electron production, surface photochemistry, and solar energy harvesting with plasmonic nanoparticles [111–118]. In the case of the propagating surface or localized plasmons in individual nanostructures, the plasmon decay is due to the excitations involving the 3D continua of the bulk bands. With present results we show that efficient plasmon decay can be reached owing to a single 2D continuum of the QW-localized unoccupied electronic states in the junction (single QW-localized state at  $E_0$  for the electron motion perpendicular to the surface). Since the electronic states of the metal slabs possess a discrete energy spectrum with respect to the

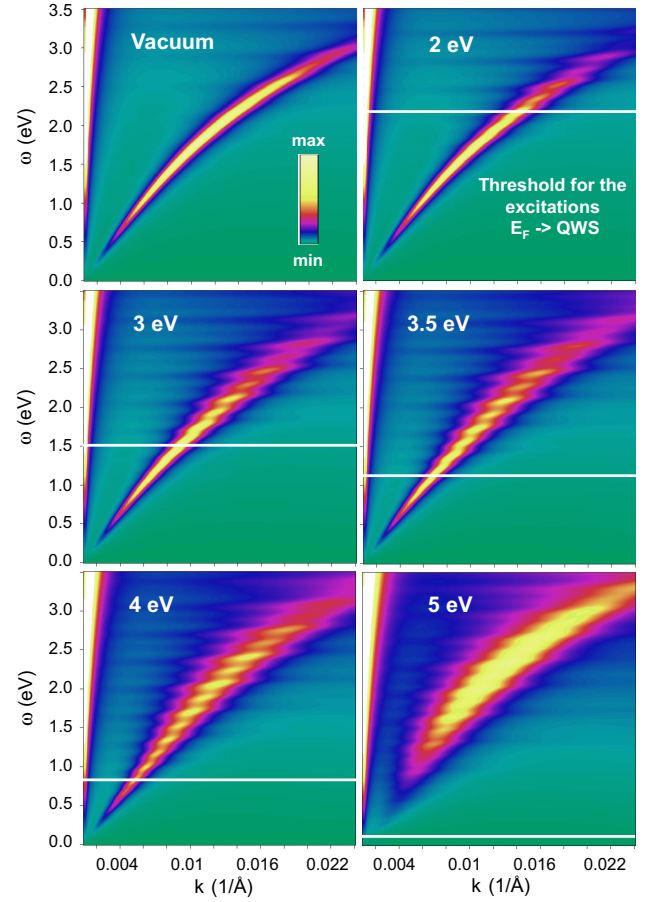


FIG. 5. Loss function calculated with RPA for the nanostructure with  $D_g = 8$  Å gap between  $L = 20$  nm Al slabs. Results are shown as functions of the wave vector  $k$  and energy  $\omega$ . Different panels of the figure correspond to the case of the vacuum gap (vacuum) and QW functionalized gap. In this latter situation the depth of the QW potential,  $V_0$ , is indicated in eV at the top left of each panel. The horizontal white lines indicate the threshold frequency  $\omega_{th}$  for the optical transitions between unoccupied QWS and metal states below Fermi level.

transverse motion, the GP broadening appears in the form of avoided crossing structures between the GP dispersion curve and discrete excitation energies [66,78,79] as nicely seen in Fig. 5. Increasing the depth of the QW shifts the energy of the QWS and consequently the threshold frequency for the plasmon broadening to lower values.

While Fig. 5 provides a qualitative picture of the effect of the QW functionalized gap on the GP, the quantitative information on the plasmon lifetime and propagation length can be deduced from the RPA results presented in Fig. 6. In Fig. 6(a) we show the frequency width  $\Delta\omega_{GP}$  (inverse of the lifetime,  $\tau^{-1}$ ) of the GP at fixed wave vector  $k_{GP}$ , and in Fig. 6(b) we show the wave vector broadening of the GP resonance  $\Delta k_{GP}$  (inverse of the propagation length,  $\ell^{-1}$ ) at fixed  $\omega_{GP}$ . Results are obtained as a function of the GP frequency  $\omega_{GP}$  by performing the fixed  $k$  and fixed  $\omega$  cuts of the RPA loss function in Fig. 5. A Fourier filter has been applied to the data. This allows us to attenuate the strongly oscillating features caused by the avoided crossings between



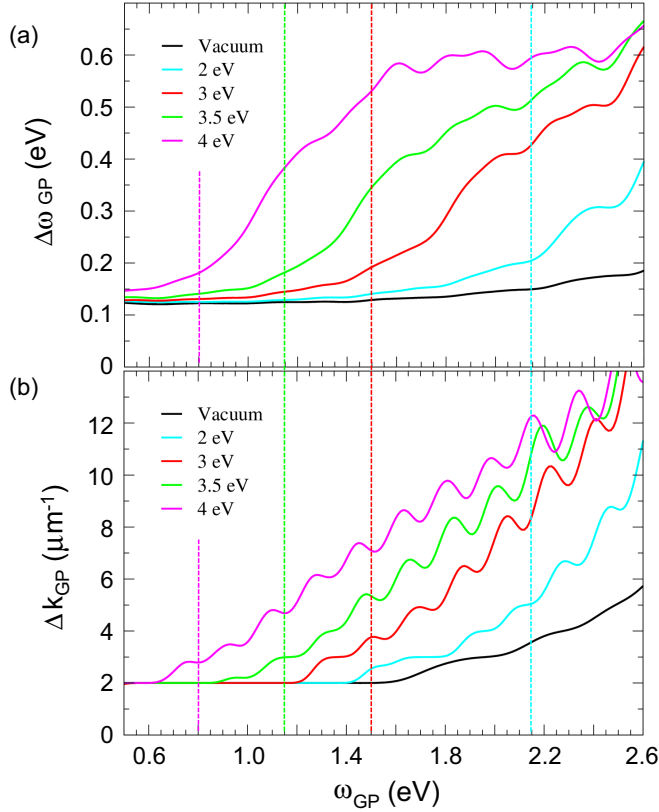


FIG. 6. The width of the gap plasmon resonance calculated with RPA for the vacuum and QW functionalized  $D_g = 8$  Å gap between  $L = 20$  nm Al slabs. Results are shown as functions of the frequency of the GP along the  $\omega_{GP}(k_{GP})$  dispersion curve. For the QW functionalized gap the calculations were performed for various depths of the QW potential  $V_0$ . The value of  $V_0$  is indicated (in eV) in the insets where the color code is explained. (a) Frequency width  $\Delta\omega_{GP}$  of the gap plasmon resonance. (b) Wave-vector width  $\Delta k_{GP}$  of the GP resonance. Vertical lines of the corresponding colors indicate the threshold frequency  $\omega_{th}$  for the optical transitions between unoccupied QWS and metal states below Fermi level.

plasmon and electron-hole excitations. Only the main trends in the plasmon broadening are thus retained. This mimics the situation of thick metal leads, where the effects of the quantization of the electron motion perpendicular to the film surface will be lifted. Note however that, even being attenuated, these oscillating features are still visible in particular in Fig. 6(b). For the completeness of the presentation we show the “raw” data for the frequency broadening of the GP later in this section (see Fig. 8).

For the vacuum gap, the RPA calculations in Fig. 6 reproduce the well-documented results [10,12–14,17,53] that can be fully retrieved with classical electromagnetic theory. At low frequencies, the GP is characterized by the frequency width  $\Delta\omega_{GP} = 0.12$  eV and wave-vector width  $\Delta k_{GP} = 2$   $\mu\text{m}^{-1}$  because of the plasmon decay via intraslab electron-hole pair excitations. The corresponding propagation length is 0.5  $\mu\text{m}$ . With increasing frequency, the electric field penetrates deeper into the metal leading to larger losses so that  $\Delta\omega_{GP}$  and  $\Delta k_{GP}$  increase. The relatively low propagation length in the present case is because of the high attenuation

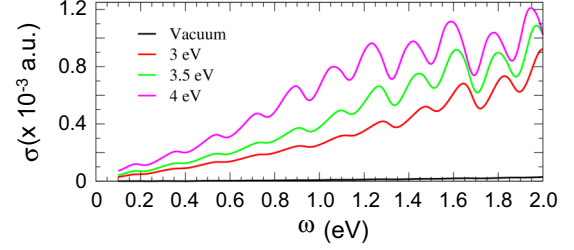


FIG. 7. Conductivity of the  $D_g = 8$  Å junction between  $L = 20$  nm Al slabs. Results are shown as functions of the frequency of the  $z$ -polarized plane wave for the vacuum and QW functionalized gaps. For the QW functionalized gap the calculations were performed for various depths of the QW potential  $V_0$  as indicated in eV in the inset where the color code is explained.

in Al and small width of the gap. Using, e.g., Ag metal slabs would strongly increase the GP lifetime and propagation length. However quantum computational study in this case requires atomistic description of metallic leads, and it is out of reach presently.

For the QW functionalized gap, a new efficient channel of the GP decay via electron-hole pair excitations into the empty QWS opens above  $\omega_{th}$ . This results in the up to four times increase of the frequency broadening,  $\Delta\omega_{GP}$  [Fig. 6(a)], and wave-vector broadening,  $\Delta k_{GP}$  [Fig. 6(b)], of the GP resonance. Correspondingly, plasmon lifetime  $\tau$  and propagation length  $\ell$  are reduced by the same factor. The finite energy width  $\Gamma$  of the quasistationary QWS (see Fig. 2) explains the absence of the sharp steplike threshold behavior at  $\omega_{GP} = \omega_{th}$ . Progressive increase of the plasmon broadening is observed starting from  $\omega_{GP} \gtrsim \omega_{th} - \Gamma$ , and the entire QWS resonance in PDOS becomes available for transitions when  $\omega_{th} + \Gamma \lesssim \omega_{GP}$ .

The frequency onset of the transitions to the QWS can be controlled by tuning the QWS energy  $E_0$ , i.e., by modifying the depth  $V_0$  of the QW potential as indicated by vertical dashed lines in Fig. 6. This opens up a possibility of the active electrical control of the decay rate and the propagation length of the GP by applying voltage to a gate electrode which in turn would shift the energy of the QWS.

### C. Model classical calculations including electron transport through the junction

The electron excitations into the QWS leading to the faster decay of the GP resonance, as found in the RPA calculations, can be linked with the transport properties of the junction. Indeed, the QWS population decays via resonant energy-conserving electron tunneling to both metal slabs. Thus, the electronic excitations into the QWS from one of the metal slabs allows for excited electrons to be transferred across the junction to the opposite slab. The QWS serves as a gateway for the PAT [67–75]. The associated local conductivity  $\sigma(\omega)$  can be obtained from the TDDFT calculations as the ratio between the current and electric field in the gap (see Sec. II). In Fig. 7 we show the absolute value of the conductivity of the  $D_g = 8$  Å junction between  $L = 20$  nm Al slabs obtained for the metal-vacuum-metal and metal-QW-metal cases. As compared to the vacuum gap, the PAT via an intermediate



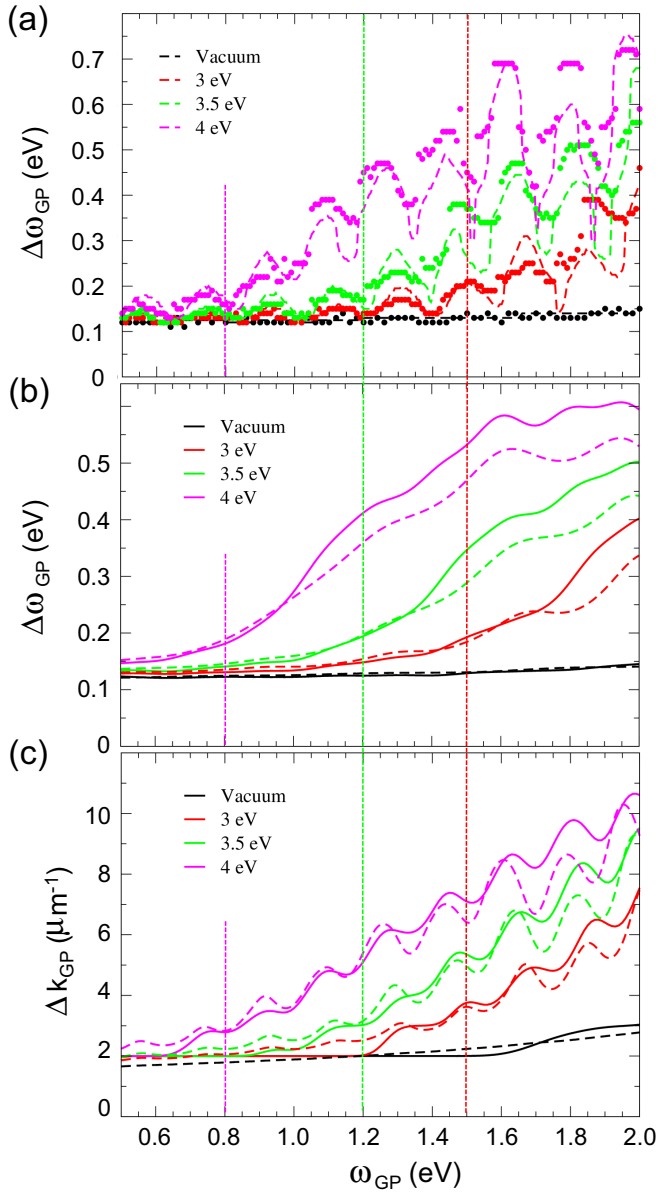


FIG. 8. The width of the gap plasmon resonance calculated with RPA [dots in (a); solid lines in (b), and (c)], and classical electromagnetic model (dashed lines) for the vacuum and QW functionalized  $D_g = 8$  Å gap between  $L = 20$  nm Al slabs. For the QW functionalized gap the calculations were performed for various depths of the QW potential  $V_0$  as indicated in the insets. Results are shown as functions of the frequency of the GP along the  $\omega_{GP}(k_{GP})$  dispersion curve. Panels (a) and (b): Frequency width  $\Delta\omega_{GP}$  of the gap plasmon resonance obtained from RPA and classical electromagnetic calculations without (a) and with (b) Fourier filter smoothing of the data. (c) Momentum broadening  $\Delta k_{GP}$  of the GP resonance. The Fourier filter is applied. Vertical dashed lines of the corresponding color indicate the threshold frequency  $\omega_{th}$  for the optical transitions between unoccupied QWS and metal states below Fermi level.

QWS resonance leads to orders of magnitude increase of the ac conductivity of the junction. This effect can be further controlled by varying the depth of the QW potential  $V_0$  and thus the energy of the QWS.

The conductivity  $\sigma(\omega)$  calculated with TDDFT allows us to define the local dielectric function of the gap  $\epsilon_g$  using Eq. (10). Thus, the PAT is represented via local classical model so that the classical electromagnetic calculations of the plasmon modes using Eq. (11) can be performed. In Figs. 8(a)–8(c) we compare the model classical and RPA results for the frequency  $\Delta\omega_{GP}$  (inverse of the lifetime) and the momentum  $\Delta k_{GP}$  (inverse of the propagation length) width of the GP resonance as function of the GP frequency  $\omega_{GP}$ . The agreement between the two approaches is remarkable. Even the features in the RPA data because of the avoided crossing structures between plasmon and electron-hole pair excitations are well reproduced within the classical approach. It is worth mentioning that at higher frequencies, above the range shown in Fig. 8, the classical model fails. This is primarily because the dynamics of the excited population in the QW localized quasistationary electronic state prevents reliable extraction of the local transport properties of the junction.

With results shown in Fig. 8, the faster decay and shorter propagation length of the GP in the QW functionalized gap can be thus explained in classical terms as caused by the resistive losses associated with ac electron transport via an intermediate of the QWS. This establishes a quantum-classical correspondence for PAT via a gateway QWS where the electron-hole pair excitations from the metal leads into the QWS are linked with resistive electron transport through the junction. Importantly, the frequency dependence of ac electron tunneling in this case is in sheer contrast with electron tunneling through the vacuum gaps broadly discussed in the previous works [57–66]. The PAT through the gateway gap-localized electronic states is characterized by the frequency threshold behavior absent for the electron tunneling through the nonfunctionalized gaps. As a consequence, the spatial and temporal decay of the GP owing to PAT is strongly increased above  $\omega_{th}$ . Modifying the energy of the QWS opens up a possibility to control  $\omega_{th}$  and thus the propagation length of the GP. In turn, this can be used for the amplitude variation of the GP signal between emitter and receiver along the plasmonic circuit.

Since the RPA calculations are time consuming, studying dependence of the results on different parameters of the junction would require prohibitively long computation times. Our finding that the PAT can be accounted for within the classical model allows us to notably reduce the computational effort. Thus, we use classical electromagnetic calculations to analyze how the GP decay in the functionalized gap depends on the width of the junction, i.e., on the electronic coupling between QWS and metal slabs. In Figs. 9(a) and 9(b) we show the classical model results for the frequency  $\Delta\omega_{GP}$  (inverse of the lifetime) and the momentum  $\Delta k_{GP}$  (inverse of the propagation length) width of the GP resonance as a function of the GP frequency  $\omega_{GP}$ . The calculations are performed for the  $D_g = 10$  Å junction between  $L = 20$  nm Al slabs. Qualitatively, the main features are similar to those obtained for narrower gap  $D_g = 8$  Å (Figs. 6 and 8). In particular, as compared to the vacuum junction, the PAT through the QWS in a QW functionalized gap leads to the faster decay in time of the GP plasmon and its shorter propagation length above the threshold frequency  $\omega_{th}$ . The latter depends on the depth of the QW potential  $V_0$ .

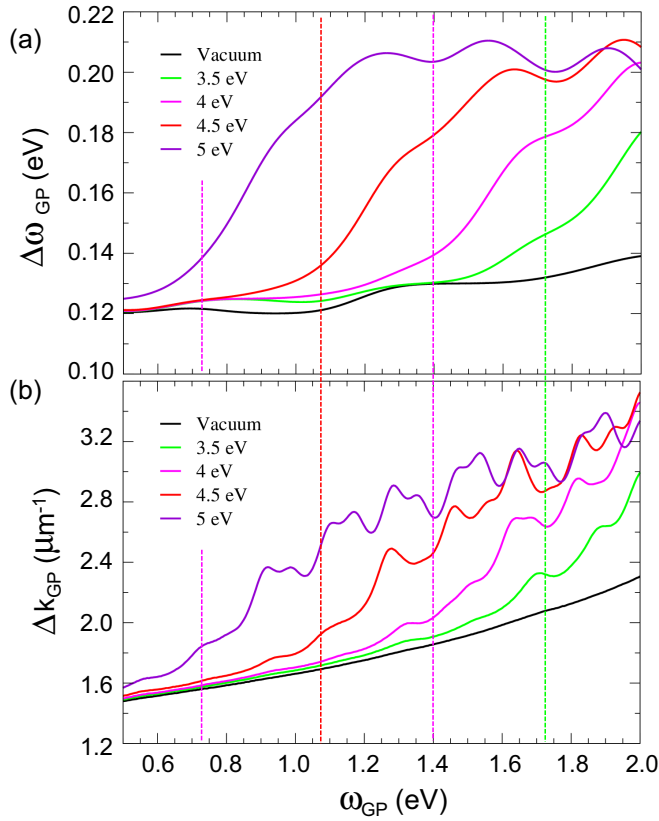


FIG. 9. The width of the gap plasmon resonance calculated with classical model approach for the vacuum and QW functionalized  $D_g = 10$  Å gap between  $L = 20$  nm Al slabs. Results are shown as functions of the frequency of the GP along the  $\omega_{GP}(k_{GP})$  dispersion curve. For the QW functionalized gap the calculations were performed for various depths of the QW potential  $V_0$ . It is indicated in eV in the insets where the color code is explained. (a) Frequency width  $\Delta\omega_{GP}$  of the gap plasmon resonance. (b) Wave-vector width  $\Delta k_{GP}$  of the GP. Vertical dashed lines of the corresponding color indicate the threshold frequency  $\omega_{th}$  for the optical transitions between unoccupied QWS and metal states below Fermi level. The Fourier filter is applied to attenuate the structures linked with avoided crossing between plasmon and single-particle excitations.

The difference with the  $D_g = 8$  Å case is however clearly reflected by the sharper threshold behavior at  $\omega_{GP} = \omega_{th}$  and essentially smaller effect of the PAT on the GP decay above the threshold. For  $D_g = 8$  Å the decay rate and propagation length of the GP are varied by nearly a factor of 4, while for  $D_g = 10$  Å only about 60% variation is obtained. This is because larger width of the junction results in the broader tunneling barriers at metal/QW interfaces. Coupling of the QWS to the metal slabs is reduced. The QWS resonance in projected density of electronic states narrows (Fig. 2) which explains sharper threshold behavior. As a second consequence of the reduced QWS-metal coupling, the ac conductivity of the junction decreases so that the effect of PAT becomes smaller. However, choosing metal leads with lower attenuation should reduce the “reference” GP width obtained for the vacuum gap or functionalized gap below the frequency threshold for PAT. Thus, the relative importance of the plasmon broadening owing to PAT above  $\omega_{th}$  might be increased.

This discussion brings about an important point concerning the robustness of the present results. As we have shown, the change of the GP energy and momentum broadening above the threshold frequency due to the PAT effect is associated with appearance of an additional decay channel. It consists in the excitation of electrons from the valence bands into the QWS, and depends on the corresponding couplings. The tails of the valence-band wave functions into the gap region are mainly determined by the metal work function and dielectric spacer layers. Therefore, the valence-band electron coupling with the QWS is only slightly sensitive to the specific band structure of the metal leads. Thus, while obtained with model Al metal, the results reported here should qualitatively hold for widely used plasmonic metals such as gold and silver.

One comment is in order with respect to the size of the junction needed for observable effects. *A priori*, the coupling between the QW structure and metal leads can be controlled using the oxide layers as metal/QW interfaces [119,120]. In the case of the vacuum layers between metal surfaces and QW structure as considered here, the tunneling barrier is determined by the binding energy of the QWS with respect to the vacuum level. At variance, in the case of the oxide film, the energy should be referred with respect to the bottom of the oxide conduction band. This allows much larger  $D_g$  to be used while keeping the same ac conductivity of the junction. Additionally, for self-organized molecular layers in the junction, the strength of the coupling between LUMO and metal leads can be controlled by the choice of the molecular end groups [121–126].

#### IV. SUMMARY AND CONCLUSIONS

In summary, using quantum RPA, TDDFT, and classical model calculations we have studied the effect of the optically assisted transport on the gap plasmon in a compound nanoscale device. With the example of a QW structure sandwiched in a nanometer vacuum gap between two 20-nm-thick metal slabs, we have shown that the temporal and spatial decay of the gap plasmon can be strongly affected by the presence of the unoccupied 2D band of QW localized electronic states in the junction. In the studied case, the coupling between collective excited mode of the system (gap plasmon) and single-particle electron-hole pair excitations from metal surfaces into the QW-localized electronic states leads to the strong decay of the gap plasmon above a threshold frequency. This threshold frequency can be modified by changing the energy of the bottom of the QW continuum which opens up a possibility of active electrical control using a gate electrode.

One can imagine a device where the signal is transmitted via the gap plasmon from an emitter to detector in the functionalized gap between metal surfaces. Depending on the controllable energy of the unoccupied gap-localized electronic state, the gap plasmon propagation length can be altered so that the amplitude of the transmitted signal can be strong or exponentially weak.

We have demonstrated that the RPA results for the dispersion and broadening of the gap plasmon can be retrieved using classical Maxwell equations. To this end, the photoassisted transport across the junction has to be taken into account, e.g., using a local effective-medium description of the junction as

proposed in this work. The good agreement between classical and RPA results for the functionalized gap allows us to link electronic excitations into the resonant QWS and transport properties of the junction. The ac electron transport through the gateway gap-localized electronic states, and the associated losses, are the main physical mechanisms behind the plasmon broadening. Along with earlier works on electron tunneling in vacuum gaps, the possibility of the classical treatment of the resonant PAT effect on the gap plasmon is very attractive as it opens a way to address complex systems with large sizes where the quantum approach is impossible.

Despite that the present work has been performed for a model structure, our main results reflect the robust physics of the GP decay via electronic excitations from the valence band of the metal leads into the unoccupied electronic states localized in the functionalized gap. In particular, we have shown that even a single quantum well localized state quantized in the direction perpendicular to the structure (2D QWS continuum vs 3D bulk bands of metal if the motion parallel to the surface is considered) can lead to a sizable reduction of the gap plasmon lifetime and propagation length above the thresh-

old frequency. Clearly, subject to specific conditions, these results should hold for different functionalized plasmonic gaps. In this respect, we hope that our work will stimulate quantum studies of the transport properties of molecule functionalized gaps. Albeit extremely heavy computationally, this might reveal further interesting aspects of the coupling between propagating plasmons, electron transport, and excited states in such systems [127].

The sensitivity of the gap plasmons to the ac electron transport properties reported here opens further perspectives in design of nanosensors and integrated active optical devices.

## ACKNOWLEDGMENTS

V.M.S. acknowledges support from the Basque Government (Grant No. IT-756-13 UPV/EHU) and the Spanish Ministry of Economy, Industry and Competitiveness (MINEICO) (Grant No. FIS2016-76617-P). V.M.S. and A.K.K. acknowledges Project No. PI2017-30 of the Department of Education of the Basque Government.

- 
- [1] J. A. Schuller, E. S. Barnard, W. Cai, Y. C. Jun, J. S. White, and M. L. Brongersma, *Nat. Mater.* **9**, 193 (2010).
  - [2] B. Lukyanchuk, N. I. Zheludev, S. A. Maier, N. J. Halas, P. Nordlander, H. Giessen, and C. T. Chong, *Nat. Mater.* **9**, 707 (2010).
  - [3] M. I. Stockman, *Opt. Express* **19**, 22029 (2011).
  - [4] P. Biagioni, J.-S. Huang, and B. Hecht, *Rep. Prog. Phys.* **75**, 024402 (2012).
  - [5] M. Kauranen and A. V. Zayats, *Nat. Photon.* **6**, 737 (2012).
  - [6] C. Chicanne, T. David, R. Quidant, J. C. Weeber, Y. Lacroute, E. Bourillot, A. Dereux, G. Colas des Francs, and C. Girard, *Phys. Rev. Lett.* **88**, 097402 (2002).
  - [7] Y. Babayan, J. M. McMahon, S. Li, S. K. Gray, G. C. Schatz, and T. W. Odom, *ACS Nano* **3**, 615 (2009).
  - [8] F.-P. Schmidt, H. Dittlbacher, U. Hohenester, A. Hohenau, F. Hofer, and J. R. Krenn, *Nat. Commun.* **5**, 3604 (2014).
  - [9] A. Campos, A. Arbouet, J. Martin, D. Gérard, J. Proust, J. Plain, and M. Kociak, *ACS Photon.* **4**, 1257 (2017).
  - [10] J. Jung, T. Søndergaard, and S. I. Bozhevolnyi, *Phys. Rev. B* **79**, 035401 (2009).
  - [11] R. Esteban, T. V. Teperik, and J. J. Greffet, *Phys. Rev. Lett.* **104**, 026802 (2010).
  - [12] M. G. Nielsen, A. Pors, O. Albrechtsen, and S. I. Bozhevolnyi, *Opt. Express* **20**, 13311 (2012).
  - [13] J. Yang, C. Sauvan, A. Jouanin, S. Collin, J.-L. Pelouard, and P. Lalanne, *Opt. Express* **20**, 16880 (2012).
  - [14] C. Belacel, B. Habert, F. Bigourdan, F. Marquier, J.-P. Hugonin, S. Michaelis de Vasconcellos, X. Lafosse, L. Coolen, C. Schwob, C. Javaux *et al.*, *Nano Lett.* **13**, 1516 (2013).
  - [15] J. B. Lassiter, F. McGuire, J. J. Mock, C. Ciraci, R. T. Hill, B. J. Wiley, A. Chilkoti, and D. R. Smith, *Nano Lett.* **13**, 5866 (2013).
  - [16] T. B. Hoang, G. M. Akselrod, C. Argyropoulos, J. Huang, D. R. Smith, and M. H. Mikkelsen, *Nat. Commun.* **6**, 7788 (2015).
  - [17] Y. Yang, O. D. Miller, T. Christensen, J. D. Joannopoulos, and M. Soljačić, *Nano Lett.* **17**, 3238 (2017).
  - [18] E. N. Economou, *Phys. Rev.* **182**, 539 (1969).
  - [19] R. Zia, M. D. Selker, P. B. Catrysse, and M. L. Brongersma, *J. Opt. Soc. Am. A* **21**, 2442 (2004).
  - [20] S. I. Bozhevolnyi and J. Jung, *Opt. Express* **16**, 2676 (2008).
  - [21] A. Wiener, A. I. Fernández-Domínguez, J. B. Pendry, A. P. Horsfield, and S. A. Maier, *Opt. Express* **21**, 27509 (2013).
  - [22] S. Raza, T. Christensen, M. Wubs, S. I. Bozhevolnyi, and N. A. Mortensen, *Phys. Rev. B* **88**, 115401 (2013).
  - [23] A. Moreau, C. Ciraci, and D. R. Smith, *Phys. Rev. B* **87**, 045401 (2013).
  - [24] J. Benedicto, R. Pollès, C. Ciraci, E. Centeno, D. R. Smith, and A. Moreau, *J. Opt. Soc. Am. A* **32**, 1581 (2015).
  - [25] C. Ciraci, M. Scalora, and D. R. Smith, *Phys. Rev. B* **91**, 205403 (2015).
  - [26] S. I. Bozhevolnyi, V. S. Volkov, E. Devaux, J.-Y. Laluet, and T. W. Ebbesen, *Nature (London)* **440**, 508 (2006).
  - [27] H. Choo, M.-K. Kim, M. Staffaroni, T. J. Seok, J. Bokor, S. Cabrini, P. J. Schuck, M. C. Wu, and E. Yablonovitch, *Nat. Photon.* **6**, 838 (2012).
  - [28] K. C. Y. Huang, M.-K. Seo, T. Sarmiento, Y. Huo, J. S. Harris, and M. L. Brongersma, *Nat. Photon.* **8**, 244 (2014).
  - [29] C. L. C. Smith, N. Stenger, A. Kristensen, N. A. Mortensen, and S. I. Bozhevolnyi, *Nanoscale* **7**, 9355 (2015).
  - [30] B. Pettinger, K. F. Domke, D. Zhang, G. Picardi, and R. Schuster, *Surf. Sci.* **603**, 1335 (2009).
  - [31] Z. Zhang, S. Sheng, R. Wang, and M. Sun, *Anal. Chem.* **88**, 9328 (2016).
  - [32] R. Zhang, Y. Zhang, Z. C. Dong, S. Jiang, C. Zhang, L. G. Chen, L. Zhang, Y. Liao, J. Aizpurua, Y. Luo *et al.*, *Nature (London)* **498**, 82 (2013).
  - [33] R. Berndt, J. K. Gimzewski, and P. Johansson, *Phys. Rev. Lett.* **67**, 3796 (1991).
  - [34] P. Johansson, R. Monreal, and P. Apell, *Phys. Rev. B* **42**, 9210 (1990).



- [35] G. Schull, N. Néel, P. Johansson, and R. Berndt, *Phys. Rev. Lett.* **102**, 057401 (2009).
- [36] K. Kaasbjerg and A. Nitzan, *Phys. Rev. Lett.* **114**, 126803 (2015).
- [37] P. Roelli, C. Galland, N. Piro, and T. J. Kippenberg, *Nat. Nanotechnol.* **11**, 164 (2015).
- [38] C. Sauvan, J. P. Hugonin, I. S. Maksymov, and P. Lalanne, *Phys. Rev. Lett.* **110**, 237401 (2013).
- [39] J. Galego, F. J. García-Vidal, and J. Feist, *Phys. Rev. X* **5**, 041022 (2015).
- [40] C. Tserkezis, R. Esteban, D. O. Sigle, J. Mertens, L. O. Herrmann, J. J. Baumberg, and J. Aizpurua, *Phys. Rev. A* **92**, 053811 (2015).
- [41] F. Benz, M. K. Schmidt, A. Dreismann, R. Chikkaraddy, Y. Zhang, A. Demetriadou, C. Carnegie, H. Ohadi, B. de Nijs, R. Esteban *et al.*, *Science* **354**, 726 (2016).
- [42] R. Chikkaraddy, B. de Nijs, F. Benz, S. J. Barrow, O. A. Scherman, E. Rosta, A. Demetriadou, P. Fox, O. Hess, and J. J. Baumberg, *Nature (London)* **535**, 127 (2016).
- [43] T. Neuman, R. Esteban, D. Casanova, F. J. García-Vidal, and J. Aizpurua, *Nano Lett.* **18**, 2358 (2018).
- [44] Z. C. Dong, X. L. Zhang, H. Y. Gao, Y. Luo, C. Zhang, L. G. Chen, R. Zhang, X. Tao, Y. Zhang, J. L. Yang *et al.*, *Nat. Photon.* **4**, 50 (2009).
- [45] S.-E. Zhu, Y.-M. Kuang, F. Geng, J.-Z. Zhu, C.-Z. Wang, Y.-J. Yu, Y. Luo, Y. Xiao, K.-Q. Liu, Q.-S. Meng *et al.*, *J. Am. Chem. Soc.* **135**, 15794 (2013).
- [46] T. Lutz, C. Große, C. Dette, A. Kabakchiev, F. Schramm, M. Ruben, R. Gutzler, K. Kuhnke, U. Schlickum, and K. Kern, *Nano Lett.* **13**, 2846 (2013).
- [47] M. C. Chong, L. Sosa-Vargas, H. Bulou, A. Boeglin, F. Scheurer, F. Mathevet, and G. Schull, *Nano Lett.* **16**, 6480 (2016).
- [48] Y. Zhang, Y. Luo, Y. Zhang, Y.-J. Yu, Y.-M. Kuang, L. Zhang, Q.-S. Meng, Y. Luo, J.-L. Yang, Z.-C. Dong *et al.*, *Nature (London)* **531**, 623 (2016).
- [49] C. Große, P. Merino, A. Rosławska, O. Gunnarsson, K. Kuhnke, and K. Kern, *ACS Nano* **11**, 1230 (2017).
- [50] H. Imada, K. Miwa, M. Imai-Imada, S. Kawahara, K. Kimura, and Y. Kim, *Phys. Rev. Lett.* **119**, 013901 (2017).
- [51] T. Wang and C. A. Nijhuis, *Appl. Mater. Today* **3**, 73 (2016).
- [52] B. Doppagne, M. C. Chong, E. Lorchat, S. Berciaud, M. Romeo, H. Bulou, A. Boeglin, F. Scheurer, and G. Schull, *Phys. Rev. Lett.* **118**, 127401 (2017).
- [53] J. M. Pitarke, V. M. Silkin, E. V. Chulkov, and P. M. Echenique, *Rep. Prog. Phys.* **70**, 1 (2007).
- [54] T. V. Teperik, P. Nordlander, J. Aizpurua, and A. G. Borisov, *Phys. Rev. Lett.* **110**, 263901 (2013).
- [55] A. I. Fernández-Domínguez, A. Wiener, F. J. García-Vidal, S. A. Maier, and J. B. Pendry, *Phys. Rev. Lett.* **108**, 106802 (2012).
- [56] O. Schnitzer, V. Giannini, R. V. Craster, and S. A. Maier, *Phys. Rev. B* **93**, 041409 (2016).
- [57] J. Zuloaga, E. Prodan, and P. Nordlander, *Nano Lett.* **9**, 887 (2009).
- [58] D. C. Marinica, A. K. Kazansky, P. Nordlander, J. Aizpurua, and A. G. Borisov, *Nano Lett.* **12**, 1333 (2012).
- [59] D. Xiang, J. Wu, and R. Gordon, *Nano Lett.* **17**, 2584 (2017).
- [60] J. A. Scholl, A. García-Etxarri, A. L. Koh, and J. A. Dionne, *Nano Lett.* **13**, 564 (2013).
- [61] W. Zhu and K. B. Crozier, *Nat. Commun.* **5**, 5228 (2014).
- [62] K. J. Savage, M. M. Hawkeye, R. Esteban, A. G. Borisov, J. Aizpurua, and J. J. Baumberg, *Nature (London)* **491**, 574 (2012).
- [63] H. Cha, J. H. Yoon, and S. Yoon, *ACS Nano* **8**, 8554 (2014).
- [64] H. Jung, H. Cha, D. Lee, and S. Yoon, *ACS Nano* **9**, 12292 (2015).
- [65] M. Barbry, P. Koval, F. Marchesin, R. Esteban, A. G. Borisov, J. Aizpurua, and D. Sánchez-Portal, *Nano Lett.* **15**, 3410 (2015).
- [66] A. Varas, P. García-González, J. Feist, F. J. García-Vidal, and A. Rubio, *Nanophotonics* **5**, 409 (2016).
- [67] M. Grifoni and P. Hänggi, *Phys. Rep.* **304**, 229 (1998).
- [68] G. Platero and R. Aguado, *Phys. Rep.* **395**, 1 (2004).
- [69] J. Iñarrea, G. Platero, and C. Tejedor, *Phys. Rev. B* **50**, 4581 (1994).
- [70] H. C. Liu, *Phys. Rev. B* **43**, 12538 (1991).
- [71] D. Sokolovski, *Phys. Rev. B* **37**, 4201 (1988).
- [72] M. H. Pedersen and M. Büttiker, *Phys. Rev. B* **58**, 12993 (1998).
- [73] A. Keller, O. Atabek, M. Ratner, and V. Mujica, *J. Phys. B* **35**, 4981 (2002).
- [74] M. Galperin and A. Nitzan, *Phys. Chem. Chem. Phys.* **14**, 9421 (2012).
- [75] M. Galperin and A. Nitzan, *Phys. Rev. Lett.* **95**, 206802 (2005).
- [76] R. Arielly, A. Ofarim, G. Noy, and Y. Selzer, *Nano Lett.* **11**, 2968 (2011).
- [77] H. J. Yoon, K.-C. Liao, M. R. Lockett, S. W. Kwok, M. Baghbanzadeh, and G. M. Whitesides, *J. Am. Chem. Soc.* **136**, 17155 (2014).
- [78] E. Prodan, P. Nordlander, and N. J. Halas, *Nano Lett.* **3**, 1411 (2003).
- [79] E. Prodan, P. Nordlander, and N. J. Hallas, *Chem. Phys. Lett.* **368**, 94 (2003).
- [80] A. Manjavacas, J. G. Liu, V. Kulkarni, and P. Nordlander, *ACS Nano* **8**, 7630 (2014).
- [81] J. R. M. Saavedra, A. Asenjo-Garcia, and F. J. García de Abajo, *ACS Photon.* **3**, 1637 (2016).
- [82] A. M. Brown, R. Sundararaman, P. Narang, W. A. Goddard, and H. A. Atwater, *ACS Nano* **10**, 957 (2016).
- [83] T.-C. Chiang, *Surf. Sci. Rep.* **39**, 181 (2000).
- [84] P. Dowben, *Surf. Sci. Rep.* **40**, 151 (2000).
- [85] V. E. Babicheva, M. Y. Shalaginov, S. Ishii, A. Boltasseva, and A. V. Kildishev, *Opt. Express* **23**, 31109 (2015).
- [86] I. Avrutsky, I. Salakhutdinov, J. Elser, and V. Podolskiy, *Phys. Rev. B* **75**, 241402 (2007).
- [87] A. Husakou and J. Herrmann, *Phys. Rev. Lett.* **99**, 127402 (2007).
- [88] A. Mirone, M. Idir, P. Dhez, G. Soullie, and A. Erko, *Opt. Commun.* **111**, 191 (1994).
- [89] *Optical Interference Coatings*, Springer Series in Optical Sciences Vol. 88, edited by N. Kaiser and H. K. Pulker (Springer, Berlin, 2003).
- [90] P. Banerjee, D. Conklin, S. Nanayakkara, T.-H. Park, M. J. Therien, and D. A. Bonnell, *ACS Nano* **4**, 1019 (2010).
- [91] F. Benz, C. Tserkezis, L. O. Herrmann, B. de Nijs, A. Sanders, D. O. Sigle, L. Pukenas, S. D. Evans, J. Aizpurua, and J. J. Baumberg, *Nano Lett.* **15**, 669 (2015).

- [92] R. M. Metzger, *Chem. Rev.* **115**, 5056 (2015).
- [93] N. D. Lang and W. Kohn, *Phys. Rev. B* **3**, 1215 (1970).
- [94] J. Zuloaga, E. Prodan, and P. Nordlander, *ACS Nano* **4**, 5269 (2010).
- [95] X. Zubizarreta, E. V. Chulkov, I. P. Chernov, A. S. Vasenko, I. Aldazabal, and V. M. Silkin, *Phys. Rev. B* **95**, 235405 (2017).
- [96] M. W. Knight, N. S. King, L. Liu, H. O. Everitt, P. Nordlander, and N. J. Halas, *ACS Nano* **8**, 834 (2013).
- [97] M. Castro-Lopez, D. Brinks, R. Sapienza, and N. F. van Hulst, *Nano Lett.* **11**, 4674 (2011).
- [98] G. Maidecchi, G. Gonella, R. Proietti Zaccaria, R. Moroni, L. Anghinolfi, A. Giglia, S. Nannarone, L. Mattera, H.-L. Dai, and M. Canepa, *ACS Nano* **7**, 5834 (2013).
- [99] B. Metzger, M. Hentschel, and G. H., *Nano Lett.* **17**, 1931 (2017).
- [100] M.-N. Su, P. D. Dongare, D. Chakraborty, Y. Zhang, C. Yi, F. Wen, W.-S. Chang, P. Nordlander, J. E. Sader, N. J. Halas *et al.*, *Nano Lett.* **17**, 2575 (2017).
- [101] W. Kohn and L. J. Sham, *Phys. Rev.* **140**, A1133 (1965).
- [102] O. Gunnarsson and B. I. Lundqvist, *Phys. Rev. B* **13**, 4274 (1976).
- [103] E. V. Chulkov, A. G. Borisov, J. P. Gauyacq, D. Sánchez-Portal, V. M. Silkin, V. P. Zhukov, and P. M. Echenique, *Chem. Rev.* **106**, 4160 (2006).
- [104] B. N. J. Persson and E. Zaremba, *Phys. Rev. B* **31**, 1863 (1985).
- [105] V. M. Silkin, A. García-Lekue, J. M. Pitarke, E. V. Chulkov, E. Zaremba, and P. M. Echenique, *Europhys. Lett.* **66**, 260 (2004).
- [106] V. M. Silkin, J. M. Pitarke, E. V. Chulkov, and P. M. Echenique, *Phys. Rev. B* **72**, 115435 (2005).
- [107] M. A. Ordal, L. L. Long, R. J. Bell, S. E. Bell, R. R. Bell, J. R. W. Alexander, and C. A. Ward, *Appl. Opt.* **22**, 1099 (1983).
- [108] M. I. Markovic and A. D. Rakic, *Appl. Opt.* **29**, 3479 (1990).
- [109] U. Hohenester and C. Draxl, *Phys. Rev. B* **94**, 165418 (2016).
- [110] D. C. Marinica, A. K. Kazansky, and A. G. Borisov, *Phys. Rev. B* **96**, 245407 (2017).
- [111] G. Baffou and R. Quidant, *Chem. Soc. Rev.* **43**, 3898 (2014).
- [112] H. A. Atwater and A. Polman, *Nat. Mater.* **9**, 865 (2010).
- [113] S. Mukherjee, F. Libisch, N. Large, O. Neumann, L. V. Brown, J. Cheng, J. B. Lassiter, E. A. Carter, P. Nordlander, and N. J. Halas, *Nano Lett.* **13**, 240 (2013).
- [114] C. Clavero, *Nat. Photon.* **8**, 95 (2014).
- [115] M. L. Brongersma, N. J. Halas, and P. Nordlander, *Nat. Nanotechnol.* **10**, 25 (2015).
- [116] S. Linic, U. Aslam, C. Boerigter, and M. Morabito, *Nat. Mater.* **14**, 567 (2015).
- [117] R. G. Hobbs, W. P. Putnam, A. Fallahi, Y. Yang, F. X. Kärtner, and K. K. Berggren, *Nano Lett.* **17**, 6069 (2017).
- [118] P. Christopher and M. Moskovits, *Annu. Rev. Phys. Chem.* **68**, 379 (2017).
- [119] Y.-C. Yeo, T.-J. King, and C. Hu, *J. Appl. Phys.* **92**, 7266 (2002).
- [120] J. Robertson, *J. Vac. Sci. Technol. A* **31**, 050821 (2013).
- [121] S. Hong, R. Reifengerger, W. Tian, S. Datta, J. Henderson, and C. Kubiak, *Superlattices Microstruct.* **28**, 289 (2000).
- [122] Y. Xue and M. A. Ratner, *Phys. Rev. B* **68**, 115407 (2003).
- [123] L. Patrone, S. Palacin, J. Charlier, F. Armand, J. P. Bourgoïn, H. Tang, and S. Gauthier, *Phys. Rev. Lett.* **91**, 096802 (2003).
- [124] N. D. Lang and C. R. Kagan, *Nano Lett.* **6**, 2955 (2006).
- [125] F. Chen, X. Li, J. Hihath, Z. Huang, and N. Tao, *J. Am. Chem. Soc.* **128**, 15874 (2006).
- [126] V. Obersteiner, D. A. Egger, and E. Zojer, *J. Phys. Chem. C* **119**, 21198 (2015).
- [127] G. Haran and L. Chuntanov, *Chem. Rev.* **118**, 5539 (2018).